The Astrophysical Journal, 838:59 (11pp), 2017 March 20 https://doi.org/10.3847/1538-4357/aa5cb8


# Solar Activity from 2006 to 2014 and Short-term Forecasts of Solar Proton Events Using the ESPERTA Model

T. Alberti[1], M. Laurenza[2], E. W. Cliver[3], M. Storini[2], G. Consolini[2], and F. Lepreti[1]
[1] Dipartimento di Fisica, Università della Calabria, Ponte P. Bucci, Cubo 31C, 87036, Rende (CS), Italy; tommaso.alberti@unical.it
[2] INAF-IAPS, Via del Fosso del Cavaliere 100, I-00133, Roma, Italy; monica.laurenza@iaps.inaf.it
[3] National Solar Observatory, Boulder, CO, USA
*Received 2016 November 11; revised 2017 January 20; accepted 2017 January 25; published 2017 March 23*

## Abstract

To evaluate the solar energetic proton (SEP) forecast model of Laurenza et al., here termed ESPERTA, we computed the input parameters (soft X-ray (SXR) fluence and ∼1 MHz radio fluence) for all ⩾M2 SXR flares from 2006 to 2014. This database is outside the 1995–2005 interval on which ESPERTA was developed. To assess the difference in the general level of activity between these two intervals, we compared the occurrence frequencies of SXR flares and SEP events for the first six years of cycles 23 (1996 September–2002 September) and 24 (2008 December–2014 December). We found a reduction of SXR flares and SEP events of 40% and 46%, respectively, in the latter period. Moreover, the numbers of ⩾M2 flares with high values of SXR and ∼1 MHz fluences (>0.1 J $m^{-2}$ and >6 × $10^5$ sfu × minute, respectively) are both reduced by ∼30%. A somewhat larger percentage decrease of these two parameters (∼40% versus ∼30%) is obtained for the 2006–2014 interval in comparison with 1995–2005. Despite these differences, ESPERTA performance was comparable for the two intervals. For the 2006–2014 interval, ESPERTA had a probability of detection (POD) of 59% (19/32) and a false alarm rate (FAR) of 30% (8/27), versus a POD = 63% (47/75) and an FAR = 42% (34/81) for the original 1995–2005 data set. In addition, for the 2006–2014 interval the median (average) warning time was estimated to be ∼2 hr (∼7 hr), versus ∼6 hr (∼9 hr), for the 1995–2005 data set.

*Key words:* methods: data analysis – Sun: activity – Sun: flares – Sun: particle emission – Sun: radio radiation – Sun: X-rays, gamma rays

## 1. Introduction

Solar energetic particle (SEP) events (defined as those that meet or exceed the Space Weather Prediction Center (SWPC) threshold of flux $J$ (>10 MeV) = 10 pr $cm^{-2}$ $s^{-1}$ $sr^{-1}$) represent a hazard in the interplanetary space and near-Earth environment. They can disrupt space operations and radio communications, damage satellite electronics, and pose a health hazard to astronauts, as well as airline passengers and crew on polar flights. The possibility of short-term forecasting of SEP events has been studied intensively in the last decades for effective mitigation of SEP event impacts. It is well known that SEP events occur in conjunction with solar flares and coronal mass ejections (CMEs), which are believed to be responsible for particle acceleration in impulsive and gradual events, respectively (e.g., Reames 1999). Different SEP forecasting models (e.g., Storini et al. 2008; Laurenza et al. 2009, and references therein) have been proposed, based on flare- and CME-related phenomena, such as soft X-ray (SXR) and low-frequency type III and type II radio bursts. For instance, the SEP prediction model Protons (Balch 1999) operated at NOAA SWPC relies on the time-integrated SXR flux, the SXR peak flux, the occurrence or non-occurrence of metric radio type II and type IV bursts, and the location of the associated flare. It was evaluated on proton events that occurred between 1986 and 2004 (Balch 2008), and gives a fair probability of detection (POD = 57%), but a high false alarm rate (FAR = 55%). Recently, Kahler & Ling (2015) derived an algorithm for a dynamic SEP event forecast to improve the Protons model. The Proton Prediction System (PPS), developed by Smart & Shea (1989), predicts the occurrence of SEP events based only on the properties of solar flares, not using the metric type II/IV radio burst occurrence as an input. A validation of PPS by Kahler et al. (2007), based on 78 ⩾ M5 X-ray flares in the period of 1997–2001 yielded approximately equal numbers of correct predictions, false predictions, and missed SEP events.

In order to increase the SEP event prediction accuracy and warning time, Laurenza et al. (2009) developed the ESPERTA model (acronym of Empirical model for Solar Proton Events Real Time Alert), based on the logistic regression analysis on three solar parameters, viz., the flare location, 1–8 Å SXR and ∼1 MHz Type III fluence (time-integrated intensity), to provide a warning within 10 minutes following the SXR peak for ⩾M2 flares (see also Laurenza et al. 2007; Storini et al. 2008; Signoretti et al. 2011).

Several other such SEP forecasting tools have recently been developed. Dierckxsens et al. (2015) determined the probability for the occurrence of an SEP event near Earth through a statistical analysis of the relationship between SEP events and properties of ⩾M1 SXR flares (intensity and longitude) and CMEs (speed and angular width) during Solar Cycle 23. Their results represent the input for the COMESEP SEP forecast technique, which has yet to be validated in terms of verification measures (POD, FAR).

In the framework of the PROTEAS project of the National Observatory of Athens (Kontogiannis et al. 2016), the FORSPEF forecasting tool has been developed (Papaioannou et al. 2015), which makes use of a homogeneous SEP database of the re-calibrated *Geostationary Operational Environmental Satellite* (*GOES*) proton data within the energy range of 6.0–243 MeV, covering the period of 1984–2003, as well as the SEP associated solar sources in terms of flare (magnitude, location) and CME (width, velocity) characteristics. FORSPEF provides the

probability of SEP occurrence based on information of solar flares with known features. Specifically, the maximum probability of SEP occurrence is obtained by folding the probabilities for a solar flare occurrence (obtained from the magnetic field observed in its associated active region) with the probabilities derived from the FORSPEF database. No validation in terms of POD and FAR of the FORSPEF scheme has been performed so far.

The UMASEP system (Núñez 2011), exploits the correlations between the sequence of first derivatives of flare SXR flux and the first derivatives of at least one differential proton flux in the energy range of 9–500 MeV, to give a warning that the >10 MeV integral channel will reach the SWPC threshold following SXR bursts of class > C7. When considering the events of solar cycles 22 and 23 of the NOAA/SWPC SEP list, UMASEP has a POD = 81% (134/166) for all well- and poorly connected events and an FAR = 34% (69/203). Winter & Ledbetter (2015) confirmed that decametric–hectometric (1–14 MHz) type III bursts that accompanied DH type II bursts were an important diagnostic for SEP event occurrence. They used a logistic regression analysis with the principal component derived from radio observations to obtain a prediction method with an FAR = 22% and a POD = 62% for the period 2010–2013.

Theoretically, as shown by Huang et al. (2012), an ensemble prediction model incorporating the complementary information of solar flares and CMEs achieves better performance than each base prediction model taken separately. Nevertheless, the optimal choice for SEP precursors should guarantee a reasonable warning time.

A good SEP forecasting tool needs to consider parameters/phenomena that can be obtained or inferred early in a solar event and which are available close to flare maximum. This timing requirement may make the use of CME-based parameters (e.g., speed) and CME-related phenomena (e.g., type II occurrence) problematic. Among the forecasting techniques satisfying this timing requirement, the method developed by Posner (2007), exploits the short transit time of relativistic electrons to forecast SEP events with a lead time of up to 1 hr. Similarly, ESPERTA provided a median warning time of ~55 minutes (computed over 19 successfully predicted events for which SEP event onset times were provided by Posner 2007) before the occurrence of an SEP event, along with reasonable verification measures (POD = 63%, FAR = 42%), for the 1995–2005 interval on which it was developed. In this paper, we evaluate the performance of ESPERTA on a newly compiled database covering the time period of 2006–2014, which encompasses the minimum between solar cycles 23 and 24 and the rise to maximum of cycle 24. The 11 year minimum and the cycle 24 maximum during this period were both characterized by unusually low solar and geomagnetic activity relative to the preceding 100 years (see Diego et al. 2010; Otkidychev & Skorbezh 2014; Singh & Tonk 2014; Prasanna Subramanian & Shanmugaraju 2016, among others). For this interval, we calculated the basic parameters used by ESPERTA and compared them to those for the 1995–2005 period used to develop the original model. Then, the forecast verification measures for the 2006–2014 interval were computed to test the robustness of model. The SEP database and the ESPERTA parameters are presented in Sections 2 and 3, respectively. Results are derived in Sections 4–5 and discussed in Section 6, where the main conclusions are drawn.

## 2. Database

Table 1 is a listing of all SEP events during the period of 2006–2014 for which the >10 MeV proton flux was ⩾10 pfu for three consecutive 5 minute intervals. Table 1 is a continuation of the compilation of such events from 1995 to 2005 in Laurenza et al. (2009). We used 5 minute proton data obtained from both *GOES* 13 and *GOES* 15 spacecraft during their operational time, choosing the data from the spacecraft with the higher measured proton intensity (http://ngdc.noaa.gov/stp/satellite/goes/dataaccess.html). The NOAA SEP event list was used as the reference, though we tried to correct for its limitations, which include the following: (1) in many cases, the SEP event originated from behind the solar limb and the associated flare emissions are partially occulted; (2) if the SEP intensity lies above 10 pfu, then any new SEP event increases are not included in the list; (3) some SEP events are included only because of short SEP increases associated with the passages of shocks at 1 astronomical unit (au) one to three days after the flare (there were no such events from 2006 to 2014); and (4) the flare associations are sometimes not obvious, and errors or questionable flare associations are included in the list. Following the procedure in Laurenza et al. (2009), each identified SEP event is associated with a visible disk flare or a behind-the-limb eruption. Proton enhancements from different solar flares are separated and attributed to a single solar event if they increase above the ⩾10 pfu threshold or by a factor of two above it. Generally, the largest SXR flare near the SEP event onset time is identified as the SEP source by considering time coincidence with fast CMEs and type II and IV bursts. A total of 36 SEP events was identified, which we divided into three groups, according to the SXR importance of the associated flare:

1. 23 SEP events associated with ⩾M2 flares,
2. 9 SEP events associated with <M2 flares, and
3. 4 farside SEP events for which no flare data are available.

To test the accuracy of our SEP event and associated flare database, we made a comparison with those proposed by Richardson et al. (2014) and Gopalswamy et al. (2014a). Both the identified SEP events and flare associations are consistent with their lists.

In Table 1, we report the 2006–2014 SEP event list (36 events) with the following columns: (1) event number, (2) flare date, (3) peak time of the SXR burst, (4) SXR burst class (in terms of the *GOES* 1–8 Å peak SXR intensity, defined as follows: classes C1-9, M1-9, and X1-9 correspond to flare peak intensities of (1–9) × $10^{-6}$, (1–9) × $10^{-5}$, and (1–9) × $10^{-4}$, respectively) (5) heliographic coordinates of the associated flare, (6) time-integrated SXR intensity, (7) SXR integration flag (see Section 2.1 for its definition), (8) time-integrated ~1 MHz *Wind*/Waves type III intensity (see Section 2.2 for the method of integration), (9) exact radio frequency used for (7), (10) warning time for 10 pfu threshold crossing (defined to be the difference between the time when the SXR reaches its maximum +10 minutes and the end of the third consecutive five minute period for which the >10 MeV SEP flux is ⩾10 pfu), (11) SEP Forecast Result (where "Hit," "Miss," "MISS" and "blank" refer to SEP events correctly predicted, SEP events with associated frontside or backside ⩾M2 SXR flares that

**Table 1**
SEP Flare List (2006–2014)

| Event Number | SXR Date | SXR Peak Time (hh:mm) | SXR Class | Hα Location | SXR Fluence ($J/m^2$) | SXR Flag | Radio Fluence (sfu × minute) | Radio Frequency (kHz) | Warning Time >10 pfu (minute) | SEP Forecast Result |
|---|---|---|---|---|---|---|---|---|---|---|
| 1 | 2006 Dec 5 | 10:35 | X9 | S07E79 | 6.12e–1 | 5 | 1.90e+6 | 916 | 1760 | Hit |
| 2 | 2006 Dec 13 | 02:39 | X3 | S05W23 | 5.88e–1 | 5 | 1.82e+7 | 916 | 31 | Hit |
| 3 | 2010 Aug 14 | 10:05 | C4 | N17W52 | 1.19e–2 | ⋯ | 1.29e+5 | 916 | ⋯ | MISS |
| 4 | 2011 Mar 7 | 20:12 | M3 | N24W59 | 1.38e–1 | 2 | 1.12e+4 | 916 | ⋯ | Miss |
| 5 | 2011 Mar 21 | (farside) | | | | | | | | |
| 6 | 2011 Jun 7 | 06:41 | M2 | S21W64 | 4.91e–2 | 5 | 1.80e+7 | 916 | 99 | Hit |
| 7 | 2011 Aug 4 | 03:57 | M9 | N15W49 | 6.07e–2 | 5 | 8.78e+6 | 916 | 158 | Hit |
| 8 | 2011 Aug 9 | 08:05 | X6 | N17W83 | 1.77e–1 | 7 | 5.71e+6 | 916 | 40 | Hit |
| 9 | 2011 Sep 22 | 11:01 | X1 | N11E74 | 4.78e–1 | 2 | 4.32e+6 | 916 | 2154 | Hit |
| 10 | 2011 Nov 26 | 07:10 | C1 | N08W49 | 1.47e–2 | ⋯ | 1.74e+5 | 916 | ⋯ | MISS |
| 11 | 2012 Jan 23 | 03:59 | M8 | N28W36 | 3.97e–2 | 5 | 5.26e+5 | 916 | ⋯ | Miss |
| 12 | 2012 Jan 27 | 18:37 | X1 | N27W71 | 2.33e–1 | 5 | 4.38e+6 | 916 | 28 | Hit |
| 13 | 2012 Mar 7 | 00:24 | X5 | N17E15 | 6.89e–1 | 5 | 2.19e+7 | 916 | 286 | Hit |
| 14 | 2012 Mar 13 | 17:41 | M7 | N18W62 | 2.65e–1 | 3 | 2.92e+6 | 916 | 29 | Hit |
| 15 | 2012 May 17 | 01:47 | M5 | N12W89 | 1.21e–1 | 5 | 9.08e+6 | 916 | 23 | Hit |
| 16 | 2012 May 27 | (farside) | | | | | | | | |
| 17 | 2012 Jun 14 | 14:35 | M1 | S17E14 | | | | | | MISS |
| 18 | 2012 Jul 6 | 23:08 | X1 | S18W50 | 5.33e–2 | 5 | 1.21e+7 | 916 | 292 | Hit |
| 19 | 2012 Jul 12 | 16:49 | X1 | S16W09 | 5.28e–1 | 3 | 7.54e+5 | 916 | 106 | Hit |
| 20 | 2012 Jul 17 | 17:15 | M1 | S17W75 | 1.86e–1 | ⋯ | 3.27e+5 | 916 | ⋯ | MISS |
| 21 | 2012 Jul 23 | (farside) | | | | | | | | |
| 22 | 2012 Aug 31 | 20:43 | C8 | S06E20 | 6.57e–2 | ⋯ | 3.19e+6 | 916 | ⋯ | MISS |
| 23 | 2012 Sep 27 | 23:57 | C3 | N08W41 | 4.19e–3 | ⋯ | 6.18e+4 | 916 | ⋯ | MISS |
| 24 | 2013 Mar 15 | 06:58 | M1 | N11E12 | | | | | | MISS |
| 25 | 2013 Apr 11 | 07:16 | M6 | N09E12 | 7.11e–2 | 5 | 3.38e+7 | 916 | 62 | Hit |
| 26 | 2013 May 15 | 01:48 | X1 | N11E51 | 1.19e–1 | 5 | 1.58e+4 | 916 | ⋯ | Miss |
| 27 | 2013 May 22 | 13:32 | M5 | N15W70 | 1.77e–1 | 3 | 5.74e+5 | 916 | 48 | Hit |
| 28 | 2013 Jun 21 | 03:14 | M2 | S16E66 | 8.11e–2 | 2 | 6.18e+4 | 916 | ⋯ | Miss |
| 29 | 2013 Sep 29 | 23:37 | C1 | N15W40 | 3.07e–3 | ⋯ | 6.94e+4 | 916 | ⋯ | MISS |
| 30 | 2013 Dec 28 | 18:02 | C9 | S18E07 | 4.80e–3 | ⋯ | 1.23e+4 | 916 | ⋯ | MISS |
| 31 | 2014 Jan 6 | (farside) | | | | | | | | |
| 32 | 2014 Jan 7 | 18:32 | X1 | S15W11 | 2.95e–1 | 5 | 7.85e+6 | 916 | 0 | Hit |
| 33 | 2014 Feb 20 | 07:55 | M3 | S15W67 | 7.38e–2 | 3 | 1.75e+6 | 916 | 55 | Hit |
| 34 | 2014 Feb 25 | 00:49 | X4 | S12E82 | 4.64e–1 | 5 | 6.83e+6 | 916 | 786 | Hit |
| 35 | 2014 Apr 18 | 13:03 | M7 | S16W41 | 1.13e–1 | 5 | 7.98e+6 | 916 | 143 | Hit |
| 36 | 2014 Sep 10 | 17:45 | X1 | N16W06 | 3.88e–1 | 5 | 3.49e+7 | 916 | 415 | Hit |

were not predicted, SEP events with associated frontside <M2 SXR flares (no prediction made), farside SEP events with associated <M2 SXR flares, respectively).

Figure 1 contains plots of all 23 SEP events that were associated with ⩾M2 SXR flares. In each plot, the dashed red line indicates the SXR peak time (+10 minute), while the next two dashed green lines refer to 10 pfu and 100 pfu threshold crossings, respectively. A blue arrow identifies the maximum of each SEP event.

In addition to the 36 SEP events with >10 MeV peak intensities ⩾10 pfu in Table 1, we identified 276 X-ray flares of class ⩾M2 using 1 minute average SXR data recorded by instruments on board the *GOES* satellite (http://spidr.ngdc.noaa.gov/spidr/index.jsp). If no Hα flare was reported, we determined flare locations using the evolution of active regions on the solar disk reported in the *Preliminary Report and Forecast of Solar Geophysical Data* (SWPC, available at http://www.sec.noaa.gov/weekly/index.html).

Finally, we used the *Wind*/WAVES (Bougeret et al. 1995) record of low-frequency (∼1 MHz) type III radio bursts (http://lep694.gsfc.nasa.gov/waves/waves.html).

Data for the period 1995–2005 were taken from Laurenza et al. (2009).

### 2.1. Time-integrated SXR Intensity

Generally, large SEP events are associated with long lasting flares, though with some exceptions (e. g., Kahler et al. 1991; Cliver 2009). Neverthless, the necessary maximization of the warning time in any reliable SEP forecast, prevents the use of the X-ray intensity integrated over the whole flare duration, that can reach hours. Laurenza et al. (2009) showed that a representative measure of the X-ray fluence, can be obtained by integrating the X-ray intensity between the one-third power point before the X-ray peak and the one-third power point after it. An exponential fit, based on the intensity values from 6 to 10 minutes after the SXR peak, was performed to obtain an estimate of the SXR fluence (between the one-third power points) in real time for bursts that did not decay to one-third peak intensity within 10 minutes. As discussed in detail in Section 3.1.2 in Laurenza et al. (2009), for about two-thirds of the ⩾M2 SXR bursts from 1995 to 2005, the intensity did not drop below the one-third power point within 10 minutes following peak intensity. Thus it was necessary to use a curve fit to extrapolate the SXR time-profile in order to estimate the SXR fluence. Laurenza et al. (2009) noted that when the ratio of the peak SXR intensity at 10 minutes following burst peak

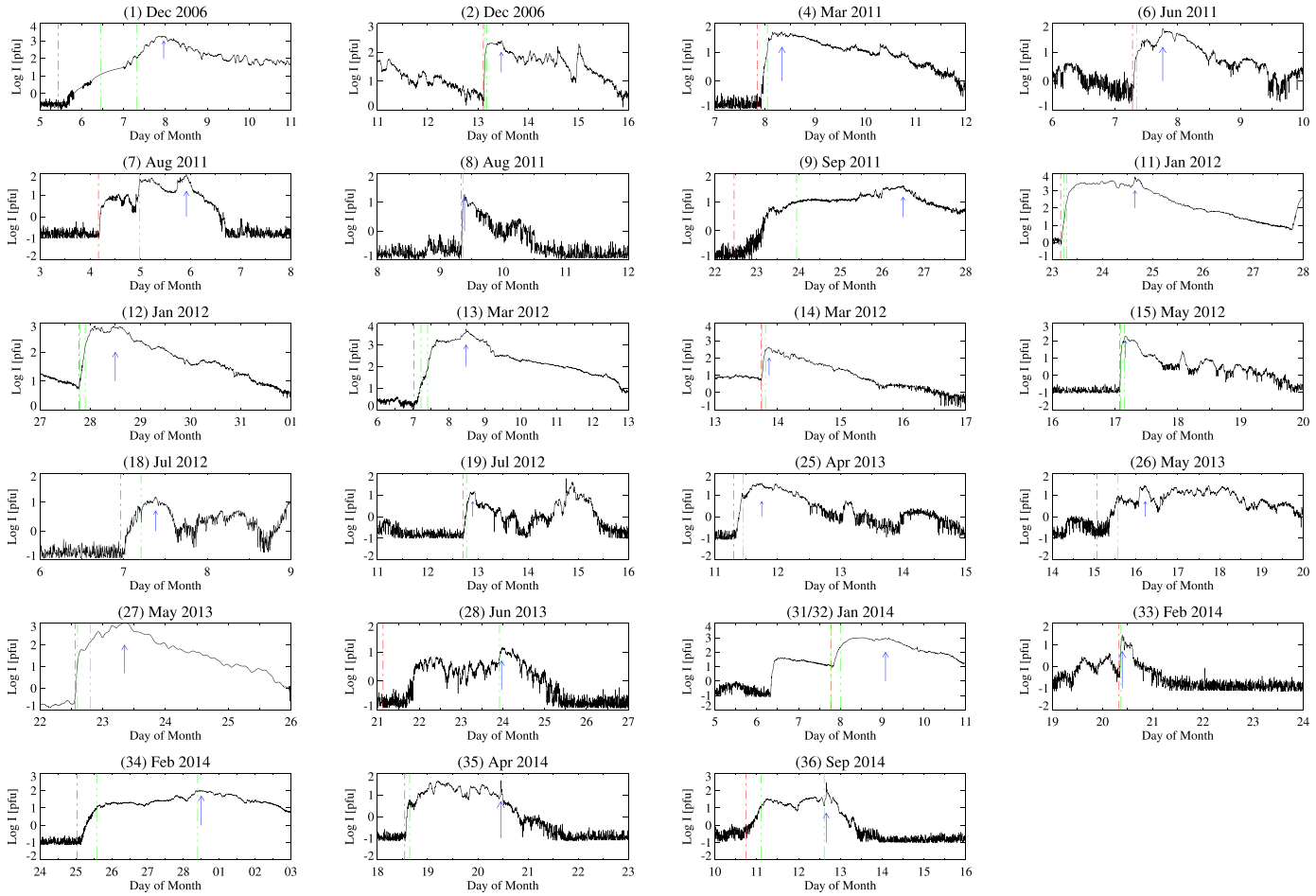


**Figure 1.** Proton flux as measured by *GOES* spacecraft for the ⩾M2 flare events in Table 1. The red line evidences the time when the forecast is made, while the next two green lines refer to 10 pfu and 100 pfu threshold crossings. Finally, a blue arrow is used to show the maximum of each event.

**Table 2**
Soft X-Ray Flare Integration Flag

| SXR Flag | $I_{10}/I_P$ Range | Value Assigned to $I_{10}/I_P$ | Decay Time to $I_{10}/I_P < 0.33$ (minutes) | Number of Cases |
|---|---|---|---|---|
| 1 | $I_{10}/I_P \geqslant 1.0$ | $I_{10}/I_P = 0.75$ | 38 | 4 |
| 2 | $0.85 < I_{10}/I_P \leqslant 0.90$ | $I_{10}/I_P = 0.85$ | 68 | 13 |
| 3 | $0.90 < I_{10}/I_P \leqslant 0.95$ | $I_{10}/I_P = 0.90$ | 104 | 11 |
| 4 | $0.95 < I_{10}/I_P < 1.0$ | $I_{10}/I_P = 0.95$ | 214 | 5 |
| 5 | $0.33 < I_{10}/I_P \leqslant 0.85$ | No Adjustments | ⋯ | 147 |
| 6 | $I_{10}/I_P \leqslant 0.33$ | No Adjustments | ⋯ | 1 |
| 7 | $I_{10}(\mathrm{d})/I_P(\mathrm{d}) \leqslant 0.33$ | No Extrapolation | ⋯ | 95 |

($I_{10}$) to the burst peak intensity ($I_P$) was >0.85 (∼15% of the sample), the calculated fluence was an over-estimate of the actual fluence. Thus they used an empirical prescription based on $I_{10}/I_P$ to reduce the fluence for such events. The SXR integration flag in column (7) of Table 1, with values from 1 to 7, specifies any empirical adjustments that were made to the curve fits depending on the value of $I_{10}/I_P$. These adjustments are specified in Table 2, which also gives the number of SXR events in each group.

### 2.2. Time-integrated 1 MHz Radio Intensity

Quoting from Laurenza et al. (2009), "The data obtained from the *Wind*/Waves website are provided in terms of ratio ($R$) of the radio flux to background with the background ($B$) provided in units of $\mu\mathrm{V/Hz}^{1/2}$. The radio flux in solar flux units (1 sfu = solar flux unit = $10^{-22}\,\mathrm{W\,m^{-2}\ Hz^{-1}}$) is then $J(\mathrm{sfu}) = 10^{10}\ (R^*B)^2/(Z_0\ \mathrm{A})$, where $Z_0$ is the characteristic impedance of free space ($Z_0 = 377\,\mathrm{W}$), and A is the area of the RAD1 antenna ($1225\,\mathrm{m}^2$)." For the 2006–2014 time interval considered, the closest frequency to 1 MHz at which measurements were usually provided was 916 kHz. Because the ∼1 MHz intensity-time curves are more irregular than the SXR time-intensity profiles, the radio integration extends from 10 minutes before the time of the SXR integration (at the one-third intensity point before the SXR peak) to 10 minutes after the X-ray peak (Laurenza et al. 2009).

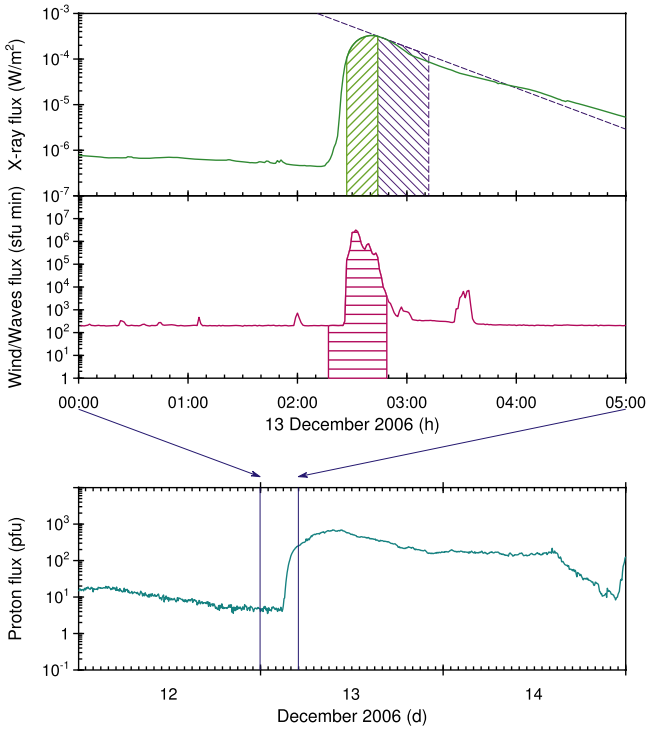


**Figure 2.** Key parameters for the 2006 December 13 SEP event. From top to bottom: X-ray flux, Radio Waves flux, and Proton flux.

An example of the computation of key parameters is illustrated in Figure 2 for the 2006 December 13 SEP event. In Figure 2, the various hatched areas refer to the different types of integration: the green area refers to SXR integration using actual data (from the one-third point before the SXR peak to 5 minutes after the SXR peak); the violet area corresponds to the integration made using the exponential fit (from 6 minutes after the peak to the one-third point after the SXR peak); and magenta area refers to radio time integration using 916 kHz channel (from 10 minutes before the one-third point on the rise of the SXR burst to 10 minutes after the SXR peak).

## 3. X-Ray and Type III Bursts Statistics

### *3.1. Comparison of Numbers and Sizes of Events During the Rise Phases of Cycles 23 (1996 September–2002 September) and 24 (2008 December–2014 December)*

In this section, we compare the SXR and radio fluences as computed in Sections 2.1 and 2.2 for SEP source flares from 2008 December–2014 December corresponding to the first six full years of solar cycle 24 (hereafter, period B) with those from the corresponding years, 1996 September–2002 September (hereafter, period A; Harvey & White 1999), for cycle 23. Current solar cycle 24 followed one of the deeper and longer 11 year minima since ~1900 (Otkidychev & Skorbezh 2014) and had one of the weakest activity maxima during this period (Richardson 2013; Singh & Tonk 2014; Wang & Colaninno 2014). We note that 63 SEP events, out of the 94 that met the SWPC threshold during cycle 23, fell within interval A, while only 34 such SEP events occurred within the corresponding years (Interval B) of solar cycle 24, a 46% reduction. Reflecting the lower rate of SEP activity in interval B, we find that the number of ⩾M2 X-ray bursts during this period (257) is 40% lower than the number (430) of such events in interval A. Nonentheless, the percentage of ⩾M2 X-ray bursts associated with SEP events is about 8%–10% in both periods (43/430 in the period A, 21/257 in the period B). The percentages of ⩾M2 X-ray bursts associated with SXR and radio fluences above two thresholds, viz., 0.1 J m$^{-2}$ for SXR and 6 × 10$^5$ sfu × minute for radio, are 26% (112/430) and 29% (125/430), respectively, for period A, versus 18% (46/257) and 21% (53/257), respectively, for Period B, indicating a ~30% decrease in these two parameters from period A to period B.

**Table 3**
Characteristics of SXR and ~1 MHz Bursts That Occurred During the First Six Years of Solar Cycle 23 (1996 September 15–2002 September 15): Number of ⩾M2 SXR Events ($N$), Median SXR Fluence ($\langle$SXR$\rangle$) with Standard Deviation (SXR$_{SD}$), Median ~1 MHz Radio Fluence ($\langle$RAD$\rangle$) with Standard Deviation (RAD$_{SD}$)

| | | SXR [J/m$^2$] | | RAD [×10$^6$ SFU × minute] | |
|---|---|---|---|---|---|
| | $N$ | $\langle$SXR$\rangle$ | SXR$_{SD}$ | $\langle$RAD$\rangle$ | RAD$_{SD}$ |
| All | 430 | 0.11 | 0.02 | 1.7 | 0.3 |
| SEP | 43 | 0.34 | 0.07 | 3.2 | 0.6 |
| Non-SEP | 387 | 0.08 | 0.01 | 1.2 | 0.2 |

**Table 4**
Characteristics of SXR and ~1 MHz Bursts That Occurred During the First Six Years of Solar Cycle 24 (2008 December 15–2014 December 15): Number of ⩾M2 SXR Events ($N$), Median SXR Fluence ($\langle$SXR$\rangle$) with Standard Deviation (SXR$_{SD}$), Median ~1 MHz Radio Fluence ($\langle$RAD$\rangle$) with Standard Deviation (RAD$_{SD}$)

| | | SXR [J/m$^2$] | | RAD [×10$^6$ SFU × minute] | |
|---|---|---|---|---|---|
| | $N$ | $\langle$SXR$\rangle$ | SXR$_{SD}$ | $\langle$RAD$\rangle$ | RAD$_{SD}$ |
| All | 257 | 0.06 | 0.01 | 1.4 | 0.4 |
| SEP | 21 | 0.17 | 0.03 | 4.4 | 0.6 |
| Non-SEP | 236 | 0.02 | 0.01 | 0.7 | 0.2 |

The above SXR and ~1 MHz parameters (number of events, median fluence, standard deviation) are listed in Tables 3 and 4 for inerval A and B, respectively. It can be seen that both the median fluences of ⩾M2 SXR and ~1 MHz radio bursts, were higher during the rise phase of cycle 23 than for the corresponding interval of cycle 24.

### *3.2. Comparison of Numbers and Sizes of Events During 1995–2005 and 2006–2014*

In this section, we compare the solar activity parameters for the 1995–2005 interval on which ESPERTA was developed (termed period C) to the corresponding data for the 2006–2014 interval (period D) on which this SEP forecast model is being evaluated. The flare data for these two intervals are given in Tables 5 and 6, respectively.

We observe that the ⩾M2 X-ray bursts occurrence is reduced by 39% in period D (276 events) with respect to period C (704 events). In addition, the percentage of ⩾M2 X-ray bursts associated with SEP events is ~9% (63/704) and 8% (23/276) for period C and period D, respectively.

When all the ⩾M2 X-ray bursts are considered, 33% (234/704) in period C are found to have an SXR fluence >0.1 J m$^{-2}$, versus 19% (53/276) in period D. A similar behavior is observed for the type III radio bursts: 36% (254/704) of all

**Table 5**
Characteristics of SXR and ∼1 MHz Bursts That Occurred During the Period 1995–2005: Number of ⩾M2 SXR Events ($N$), Median SXR Fluence ($\langle SXR \rangle$) with Standard Deviation ($SXR_{SD}$), Median ∼1 MHz Radio Fluence ($\langle RAD \rangle$) with Standard Deviation ($RAD_{SD}$)

| | | SXR [J/m$^2$] | | RAD [$\times 10^6$ SFU × minute] | |
|---|---|---|---|---|---|
| | $N$ | $\langle SXR \rangle$ | $SXR_{SD}$ | $\langle RAD \rangle$ | $RAD_{SD}$ |
| All | 704 | 0.10 | 0.03 | 1.9 | 0.4 |
| SEP | 63 | 0.31 | 0.08 | 4.1 | 0.5 |
| Non-SEP | 641 | 0.07 | 0.02 | 1.5 | 0.3 |

**Table 6**
Characteristics of SXR and ∼1 MHz Bursts That Occurred During the Period 2006–2014: Number of ⩾M2 SXR Events ($N$), Median SXR Fluence ($\langle SXR \rangle$) with Standard Deviation ($SXR_{SD}$), Median ∼1 MHz Radio Fluence ($\langle RAD \rangle$) with Standard Deviation ($RAD_{SD}$)

| | | SXR [J/m$^2$] | | RAD [$\times 10^6$ SFU × minute] | |
|---|---|---|---|---|---|
| | $N$ | $\langle SXR \rangle$ | $SXR_{SD}$ | $\langle RAD \rangle$ | $RAD_{SD}$ |
| All | 276 | 0.06 | 0.01 | 1.4 | 0.5 |
| SEP | 23 | 0.18 | 0.02 | 5.7 | 0.9 |
| Non-SEP | 253 | 0.02 | 0.01 | 0.8 | 0.3 |

events in period C (60/276, 22% in period D) are found to have a ∼1 MHz fluence $>6 \times 10^5$ SFU × minute.

We also note that both SXR and radio fluences are higher for SEP associated events, in both the time periods: the ratio between the median SXR (radio) fluence of SEP associated events and that of the non-SEP associated ones is 4.4 (2.7) and 9 (7.1) for period C and D, respectively. Note that all the ratios are higher in period D. Moreover, it is found that the median SXR fluence in period C exceeds that in period D by a factor 1.72 (3.5), when the SEP (non-SEP) associated events are considered. On the contary, the median radio fluence in period C is slightly lower (by the ratio of 0.72) than that of period D for SEP events, while for the more numerous non-SEP events the median fluence in period C is higher by a factor of 1.9.

### 3.3. Comparison of Probability Density Functions (PDFs) for 1995–2005 and 2006–2014

A SEP prediction model needs to be probabilistic, since the occurrence frequency of energetic particles has a probabilistic nature (Nymmik 1999). This requires a statistical approach to study solar flares which can/cannot generate an SEP event. Nymmik (1999) noticed that the mean SEP occurrence frequency can be described by a power-law function of the solar activity, characterized via the sunspot number, as well as the SEP size distribution. Conversely, a log-normal distribution is found to describe the SEP event particle energy spectra. Recently, Papaioannou et al. (2015), to assess the performance of the FORSPEF model, explored the conditional-probability for flares for a given active region target, under the fixed condition of the effective connected magnetic field strength (used in their model). They found that the maximum CME likelihood (peak value ∼0.27) corresponds to the flare class M2.0, indicating that the likelihood that a given flare is associated with a CME is higher for flares of class ⩾M2. Here, the PDFs associated with the SXR and the radio fluences are explored by distinguishing between SEP and non-SEP associated events. The empirical PDFs are estimated through the kernel density estimator technique (for more details, see Silverman 1998; Alberti et al. 2014). It is a non-parametric way to estimate the PDF of a time series based on the definition of a non-negative function that integrates to one and has zero mean, called the kernel function, and a smoothing parameter, termed the bandwidth. A range of kernel functions are commonly used (uniform, triangular, weighted, Epanechnikov, Gaussian) but we choose to use the Epanechnikov kernel because it is optimal in a mean square error sense such that the variance is minimized. This procedure is quite similar to the histogram method but presents some advantages such as smoothness or continuity if a suitable kernel is chosen. Moreover, we normalized the PDFs with respect to the number of events considered (see Tables 5 and 6) such that the integrated PDF over the entire range of values is equal to 1. Since the range of SXR and radio fluence values is quite different, we are not able to choose a unique binsize for both periods C and D. For instance, since the number of events is similar (between SXR and radio fluences for the same period), for the binning procedure, we choose the same number of bins for both SXR and radio PDF estimations.

Figure 3 shows the comparison between the SXR fluence PDFs obtained for period C (left panel) and period D (right panel). Generally, high values of SXR fluence are found to be associated with SEP events. We first note that the PDF associated with SEP events is shifted toward higher values compared to the non-SEP associated PDF. In particular, a critical value for the SXR fluence (0.1 J m$^{-2}$) can be identified above which the percentage of SEP associated (green line in Figure 3) ⩾M2 SXR bursts increases to 78% (49/63) and 65% (15/23) for periods C and D, respectively). In comparison, the percentage of non-SEP associated (blue line in Figure 3) ⩾M2 SXR bursts having SXR fluence greater than 0.1 J m$^{-2}$ is quite low: 29% (185/641) and 15% (38/253) for period C and D, respectively. Similar results are obtained analyzing PDFs related to 1 MHz radio fluence for both time periods. As shown in Figure 4, the percentage of SEP associated (green line) ⩾M2 X-ray bursts having radio fluence greater than $6 \times 10^5$ SFU × minute is 90% (57/63) and 83% (19/23) for periods C and D, respectively. On the other, the percentage of non-SEP associated (blue line in Figure 4) ⩾M2 X-ray bursts having radio fluence greater than $6 \times 10^5$ SFU × minute is very reduced in both periods, i.e., 31% (197/641) and 16% (41/253).

### 3.4. Solar Longitude Distribution of ⩾M2 SXR Flares With and without Associated SEP Events for 1995–2005 and 2006–2014

Finally, we investigated the longitudinal distribution associated with the location of the ⩾M2 SXR flares. Figure 5 shows the following.

1. For the period C (1995–2005), the longitudinal distribution of non-SEP associated flares is higher in the central disk region, while the longitudinal distribution of SEP associated events is higher for western events.
2. For the period D (2006–2014), a somewhat similar pattern is observed for a smaller sample of events: a clear peak for the non-SEP flares at around 0 degrees, whereas for SEP associated events, there is a comparable number of events in the longitude intervals W20°–W90° and

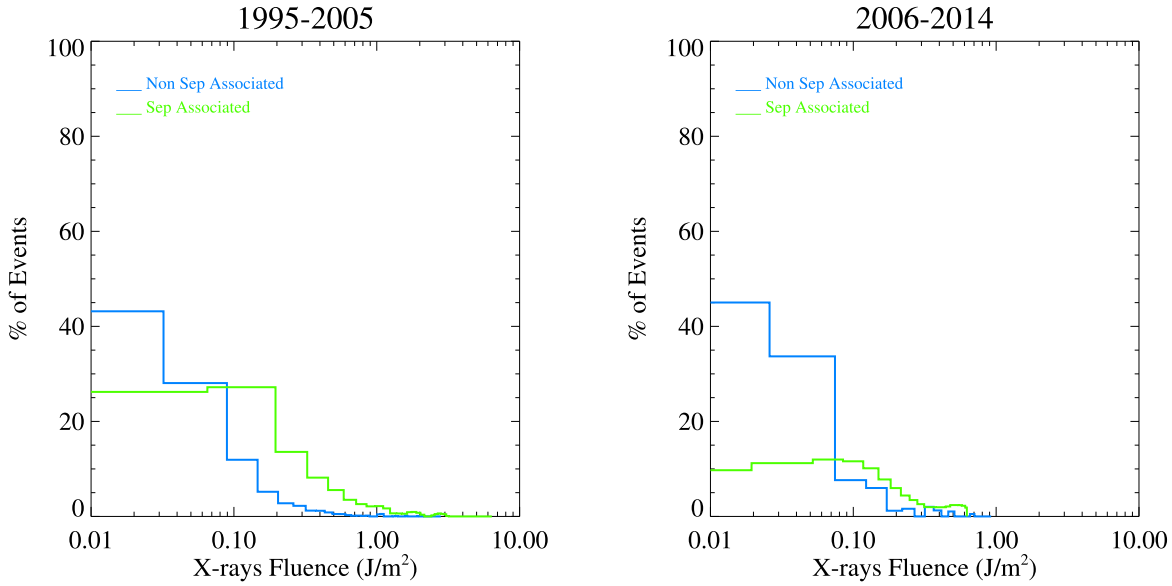


**Figure 3.** SXR fluence probability density functions: 1995–2005 database (left panel) and 2006–2014 database (right panel).

E20°–W19° (17 versus 9, respectively), though the statistics are small for the sub-groupings in longitude.

Our findings confirm the well known result that solar proton events preferentially originate in western and, to a lesser degree, central flares (e.g., Belov et al. 2005; Gopalswamy et al. 2008; Park et al. 2012). Moreover, given the noticeable presence of central solar flares associated with SEP events (especially in the 2006–2014 period), it is reasonable to invoke the contribution of fast CME-driven shock, continuously feeding accelerated particles in the magnetic field lines connecting the shock to the observer with accelerated particles (interplanetary shock dominated SEP events, Smart et al. 2006; Papaioannou et al. 2016).

## 4. Validation of ESPERTA

The model called ESPERTA, developed by Laurenza et al. (2009), is based on 1–8 Å SXR and ∼1 MHz radio fluence and flare location, to provide short-term warnings of solar energetic proton (SEP) events that meet or exceed the SWPC threshold of $J$ (>10 MeV) = 10 pr cm$^{-2}$ s$^{-1}$ sr$^{-1}$, within 10 minutes after the maximum of the associated SXR flare. ESPERTA can be applied by using the above parameters, as computed in Section 2 for period D, i.e., a new data set, independent from the interval C (1995–2005) used to develop the model. Moreover, the analysis performed in Section 3 has pointed out that the data set for period D noticeably differs from the data set in period C. Hence period D is well suited to test the accuracy and the performance of the ESPERTA model. It takes advantage of the logistic regression analysis (McCullagh & Nelder 1983, p. 98; Garcia 1994), to provide a continuous probability function for the occurrence of SEP events depending on the SXR and radio fluences for the considered ⩾M2 SXR flares. This technique is suitable for investigations, where each event is associated with a set of independent variables and characterized by a binary response (yes/no). In logistic regression technique, the probability ($P$) that an event will occur can be expressed as

$$\log\left[\frac{\text{Prob(SEPevent)}}{\text{Prob(NoSEPevent)}}\right] = \sum_{i=1}^{k} \beta_i x_i. \quad (1)$$

In our case, the probability ($P$) is a function of the chosen parameters, i.e., SXR and radio fluence ($X$ and $R$, respectively) as

$$P(\log X, \log R) = \frac{e^{\eta}}{1 + e^{\eta}} \quad (2)$$

where $\eta = \eta(\log X, \log R)$. In the ESPERTA model, the dependence of the probability by the heliographic longitude was taken into account by separating the ⩾M2 flares into three different longitude bands:

1. E 120°–E 41°
2. E 40°–W 19°
3. W 20°–W 120°.

In this way, three different values for $\eta$ corresponding to the three longitudinal bands were obtained:

1. $\eta_1 = -6.07 - 1.75\log(X) + 1.14\log(R)$- $+ 0.56\log(X)\log(R)$
2. $\eta_2 = -7.44 - 2.99\log(X) + 1.21\log(R)$- $+ 0.69\log(X)\log(R)$
3. $\eta_3 = -5.02 - 1.74\log(X) + 0.64\log(R)$- $+ 0.40\log(X)\log(R)$.

Figure 6 shows scatter plots of ∼1 MHz versus 1–8 Å SXR fluence for ⩾M2 flares that occurred during interval D for three longitude ranges on which contour plots of the SEP event probability have been drawn. It can be seen that, for each longitude range, the probability functions match the SEP event occurrence, depending on the SXR and radio fluences, as a great number of SEP events are located in the high-probability region, though not exclusively. In principle, when locating a solar flare in such diagrams, based on the SXR and radio fluence values, the probability of a following SEP event can be

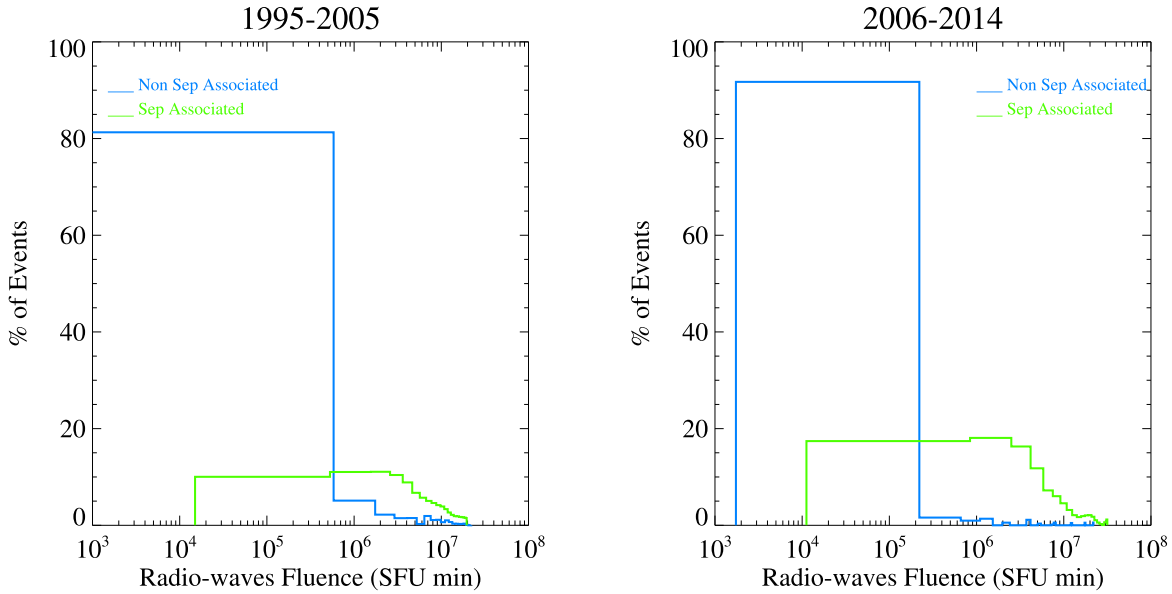


**Figure 4.** Radio fluence probability density functions: 1995–2005 database (left panel) and 2006–2014 database (right panel).

evaluated. Moreover, one probability curve can be selected to provide a yes/no result for the occurrence of an SEP event as follows. Given a ⩾M2 solar flare if the related data point is above the chosen probability contour level, a warning is given; if it is below, none is issued.

The probability curve level *Pt* used to evaluate the ESPERTA performance during 2006–2014 (dashed lines in the three scatter plots) is 28%, 28%, and 23% for western, intermediate, and eastern events respectively, which maximize the POD as discussed later.

The accuracy of the model can be investigated by evaluating the POD and the FAR, which can be expressed in terms of three values:

1. the number of hits (an SEP event was forecasted and one occurred), which we named A,
2. the number of false alarms (an SEP was forecast but none occurred), designated as *B*,
3. the number of missed events (no SEP event was predicted but one occurred), designated as C.

In this way, a relation between POD (FAR) and these parameters is obtained as

$$\mathrm{POD} = \frac{A}{A + C} \tag{3}$$

$$\mathrm{FAR} = \frac{B}{A + B}. \tag{4}$$

Moreover, we defined three other parameters: the number of correct nulls, D (no SEP event forecast and none occurred), the number of forecasts expected to be correct by chance, *E*, and the total number of forecasts (both positive and null), *N*. Using the above parameters, the following statistical quantities allow us to specify the quality of our forecast technique:

1. the percent correct, PC = *(A + D)/N*
2. the Heidke Skill Score, HSS = *(A + D–E)/(N–E)*

in which $E = [(A + B)(A + C) + (B + D)(C + D)]/N$ (Balch 2008). The number of correct forecasts by chance can be derived as $(A + C)(A + B)/N^2$ (Laurenza et al. 2009).

In order to test the efficiency and the accuracy of ESPERTA, we evaluate these statistical parameters for the database that referred to the period between 2006 and 2014. Laurenza et al. (2009) showed that for the original 1995–2005 data set, both the POD and the FAR are high (∼80%–90%) for low-probability levels (<20%), decreasing with increasing threshold, and the HSS is optimized for probabilities ranging from 20% to 40%. Nevertheless, the optimal *Pt* can be identified by maximizing the POD and HSS and minimizing the FAR. For the western ⩾M2 flares, Laurenza et al. (2009) found the optimal point to be *Pt* = 28%, versus 28% for the "intermediate" flares and 30% for eastern events. Here, for the 2006–2014 database, we confirm that the thresholds previously used are still valid for the new data set in the case of the western (POD = 61% (11/18), FAR = 35% (6/17) and intermediate events (POD = 56% (5/9), FAR = 29% (2/7)). For the small sample of eastern events, the optimization of POD, FAR, and HSS are obtained for *pt* = 23% (POD = 60 % (3/5), FAR = 0% (0/3)). These verification measures are calculated by taking into account that nine SEP events had associated disk flares with class <M2; five of these nine "MISSES," which cannot be predicted by our method, were located in the western longitude bin and four in the central one. Moreover, we evaluate the contingency matrix (which includes values of A, *B*, C, and D), by combining events from all the heliolongitude ranges. The combined results are the following: POD = 59% (19/32), FAR = 30% (8/27), HSS = 0.55 (44/80), and PC = 87% (240/276), with the probability for a chance hit = 1% (864/76176). Table 7 lists the POD and FAR values for intervals C (1995–2005) and D (2006–2014) as well as for the combined 1995–2014 period.

The similarity of the results for the three data sets shows that the performance of the method is relatively independent of the interval considered, a useful property given that, as shown in Section 3, the solar activity level for interval D was significantly lower than that during interval C.

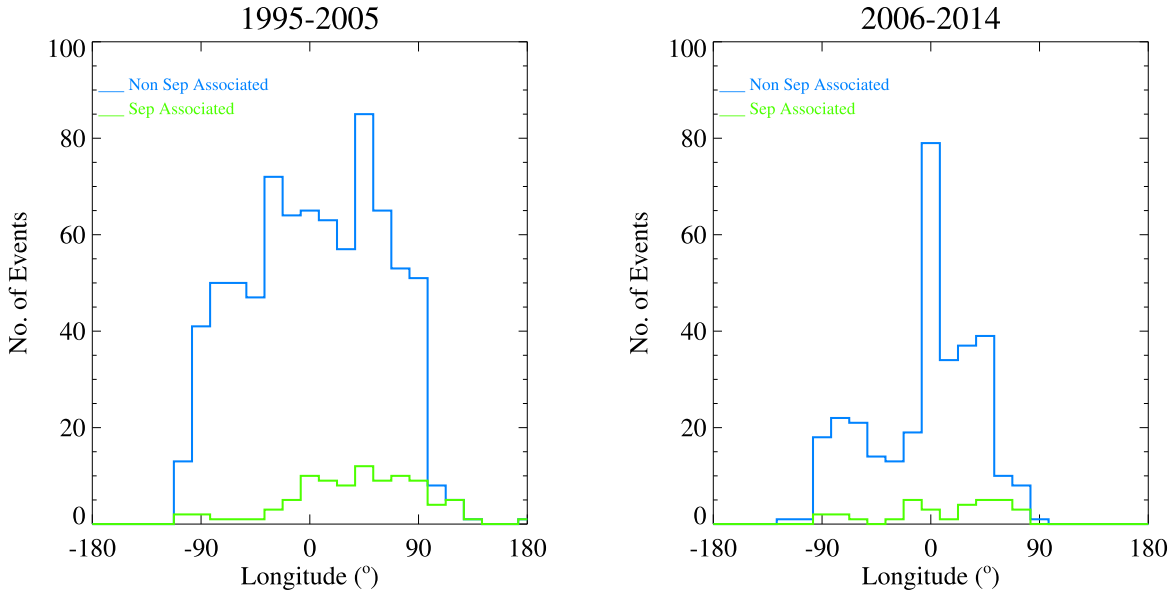


**Figure 5.** Longitudinal distributions of flare locations: 1995–2005 database (left panel) and 2006–2014 database (right panel).

## 5. Evaluation of the SEP Event Warning Times

A crucial aspect of any prediction method is the maximization of the warning time, i.e., the time difference between the SEP event start and the time when a warning is given. Since the *GOES* >10 MeV SEP time profiles, during the SEP onset period, are contaminated by relativistic electrons and protons (Posner 2007), Laurenza et al. (2009) did not determine onset times for "hit" events (made by ESPERTA) by using the *GOES* > 10 MeV SEP data but the 31–50 MeV onset times published by Posner (2007), for 19 of their "hit" events. Note that these onset times refer to the rise of the event above the pre-event background instead of the NOAA (or equivalent at 31–50 MeV) event threshold crossing. ESPERTA would have issued a lead warning time (ranging from 8 to 897 minutes and a median of 54 minute) for all the 19 events.

Here, following Núñez (2011), we calculate warning times directly from the *GOES* > 10 MeV proton fluxes, based on the difference between the time a forecast is issued (which for ESPERTA is 10 minutes after the SXR burst peak) and the time that the 10 pfu SWPC event flux threshold is reached (at the end of three consecutive 5 minute periods at or above the 10 pfu threshold). Using this definition, we obtain a median warning time of ∼4.8 hr (range from 0.4 to 52.8 hr) for our 66 hit events during the period 1995–2014. Specifically, for the 2006–2014 interval the median warning time computed on "Hit" events was estimated to be ∼2 hr (ranging from 0.4 to 35.9 hr), versus ∼6 hr (ranging from 0.8 to 52.8 hr) for the 1995–2005 data set.

For a comparison with the result of Núñez (2011), we compute the average warning time as well, that is ∼9 hr for the period 1995–2014 (∼9 hr in the 1995–2005 interval and ∼7 hr in the 2006–2014 interval), versus ∼5 hr obtained by Núñez (2011) for a study of 134 "hit" events from 1987–2006.

## 6. Discussion and Conclusions

A database of 276 SXR flares and 23 > 10 MeV SEP events that met the SWPC ⩾ 10 pfu flux threshold criterion was compiled, covering the period of 2006–2014, i.e., the declining phase of the 23rd solar cycle and the beginning part of the 24th solar cycle, in order to test the performance of ESPERTA, an SEP forecasting model developed by Laurenza et al. (2009). The ESPERTA basic parameters, i.e., 1–8 Å SXR and radio (at ∼1 MHz) fluences, were computed, by doing the time integration in real time according to the procedure proposed by Laurenza et al. (2009). The values of both parameters were obtained for the period 2006–2014 (designated interval D in this paper), and compared with those obtained for the period 1995–2005 (interval C) for which ESPERTA was developed. First, we compared the number of ⩾M2 1–8 Å SXR bursts for corresponding years, i.e., the first six years of solar cycles 23 (1996 September 15–2002 September 15, period A) and 24 (2008 December 15–2014 December 15, period B), within in periods C (1995–2005) and D (2006–2014), respectively, and found that 40% [1-(257/430)] fewer such bursts occurred during the rise phase of cycle 23 (Tables 3 and 4). Moreover, for the period A, the 26% (29%) of the selected events is above the SXR (radio) threshold (i.e., 0.1 J $m^{-2}$ for SXR, 6 × $10^5$ sfu × minute for radio); conversely, for the period B, we observe a lower percentage (18% and 21% for SXR and radio, respectively). The ⩾M2 SXR events of interval A are associated with 43 SWPC class SEP events versus 21 for interval B. These results confirm the lower occurrence rate and intensity of energetic events in the current solar cycle (cycle 24). Similar reductions were reported in the number of intensive flares (>M5.0 class) in the ascending phase of solar cycle 24 (Prasanna Subramanian & Shanmugaraju 2016), as well as in the sunspot number (Gopalswamy et al. 2014b). Moreover, Gopalswamy et al. (2015b) found a reduction in high-energy SEP events that could be attributed to several factors, such as the weak interplanetary magnetic field decreasing the efficiency of particle acceleration mechanisms. Indeed, Gopalswamy et al. (2015a) showed that a similar reduction is not observed in the overall CME rate. By a comparison of the first 73 months in solar cycles 23 and 24 (i.e., 1996 May–2002 May versus 2008 December–2014 December), they found a reduction in the sunspot number (dropped by ∼40%), while the CME rate (normalized to the sunspot number SSN) was almost the same (i.e., 0.03/SSN versus 0.05/SSN). Similarly, Gopalswamy et al. (2015b)

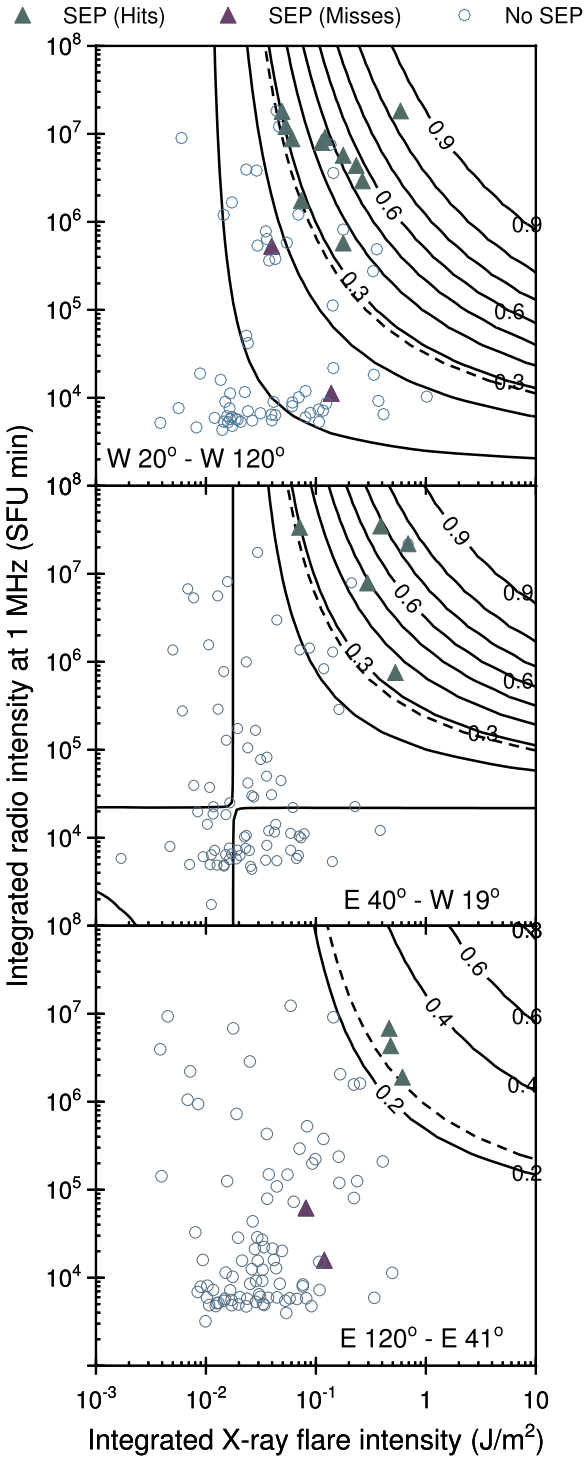


**Figure 6.** Probability contours for SEP forecasting for three different longitudinal bands: SEPs hit (green triangles), SEPs missed (violet triangles), and No SEPs associated (circles).

**Table 7**
POD and FAR Parameters

| | C 1995–2005 | D 2006–2014 | C+D 1995–2014 |
|---|---|---|---|
| POD | 63% (47/75) | 59% (19/32) | 62% (66/107) |
| FAR | 42% (34/81) | 30% (8/27) | 39% (42/108) |

showed that the distributions of CME speeds are similar in both periods (see, e.g., Gopalswamy et al. 2015b, Figure 1); conversely, the width distributions are quite different. They found that a great fraction of CMEs that occurred in solar cycle 24 was halos (∼97%), while a lower fraction (i.e., ∼75%) was observed in solar cycle 23. This can be explained in terms of a reduction in the total heliospheric pressure, producing an anomalous expansion of CMEs, allowing them to become halos. Therefore, the observed 40% reduction in SEP activity between intervals A and B cannot be due to the paucity of halo CMEs, whereas it could be accounted for by the lower large-scale magnetic activity (i.e., active regions and sunspot areas), or to the paucity of CMEs producing the seed particles. Nevertheless, the lack of CME data in our study prevents us to test these hypotheses.

The percentage of ⩾M2 SXR bursts associated with SEP events is observed to be about 8%–10% for the first six years of both cycles 23 (43/430) and 24 (21/257), consistent with past findings both for large and weak SEP events (Gopalswamy 2012; Chandra et al. 2013; Bazilevskaya et al. 2015). From a comparison of the probability distribution functions of the 1–8 Å and ∼1 MHz fluences of all ⩾M2 SXR bursts during the larger intervals C (1995–2005) and D (2006–2014), we found that the percentage of all the events exceeding the SXR fluence threshold of 0.1 J m$^{-2}$ is higher in period C than in period D (33% and 19%, respectively), as well as the percentage of all the events exceeding the radio fluence threshold of $6 \times 10^5$ sfu × minute (36% and 21%, respectively). As expected, mainly high values of both the ESPERTA basic parameters are found to be associated with SEP associated flares, in both periods C and D. The ratio between the median SXR (radio) fluence of SEP associated events and that of the non-SEP associated ones is 4.4 (2.7) and 9 (7.1) for periods C and D, respectively, though both ratios are higher in period D. In addition, the percentage of SEP associated ⩾M2 X-ray bursts above the critical value of 0.1 J m$^{-2}$ for the SXR fluence increases to 78% (70%) in period C (D), whereas the percentage of non-SEP associated ones is quite low (29% and 15% for period C and D, respectively). This finding is more apparent when the radio fluence is considered: the percentage of SEP associated ⩾M2 SXR bursts having radio fluence greater than $6 \times 10^5$ sfu × minutes is 90% (83%) for period C (D), whereas the percentage of non-SEP associated ⩾M2 flares having radio fluence greater than $6 \times 10^5$ sfu × minutes is 31% (16%). Our results show that the radio fluence is a more efficient parameter in distinguishing between the SEP associated events from the non-associated ones; this is more marked for events of period D. As a matter of fact, most of the solar sources of SEP events exhibit Type III radio emission (e.g., Duffin et al. 2015; Winter & Ledbetter 2015).

In order to test the reliability of the ESPERTA model (Laurenza et al. 2009), we evaluated the POD and the FAR of this method on a new (2006–2014) database. We found that the POD and FAR levels (59% and 30%, respectively) were comparable to those (63%, 42%) obtained for the original 1995–2005 data set, an indication of model robustness.

The ESPERTA median (average) warning time (delta between the time the forecast is issued and the time event threshold is crossed) for the 66 SEP events with peak fluxes ⩾10 pfu that were correctly called ("hits") from 1995 to 2014, was 4.8 hr (∼9 hr), in the range 0.4–52.8 hr, exceeding those

obtained by other methods (e.g., Núñez (2011) average warning time of ∼5 hr). This median (average) warning time varies from ∼2 hr (∼7 hr), ranging from 0.4 to 35.9 hr, for the 2006–2014 interval, versus ∼6 hr (∼9 hr), ranging from 0.8 to 52.8 hr for the 1995–2005 data set. We remark that it is critical to provide an SEP warning immediately after the parent solar event, given that high-energy particles may cause hazards before the integral >10MeV flux reaches the SWPC > 10 pfu threshold (Posner 2007).

All data used in this analysis are publicly accessible from NASA (*Wind*/WAVES) and NOAA (*GOES*). The *Wind*/WAVES data were obtained from ftp://solar-radio.gsfc.nasa.gov/. The SWPC SEP event list is available at http://umbra.nascom.nasa.gov/SEP/. *GOES*~SEM data have been downloaded from http://www.ngdc.noaa.gov/stp/satellite/goes/dataaccess.html. This research is partly supported by the Italian MIUR-PRIN grant 2012P2HRCR on The active Sun and its effects on Space and Earth climate. We thank the anonymous reviewer for useful suggestions.

## References

Alberti, T., Lepreti, F., Vecchio, A., et al. 2014, CliPa, 10, 1751
Balch, C. C. 1999, Radiat. Meas., 30, 231
Balch, C. C. 2008, SpWea, 6, S01001
Bazilevskaya, G. A., Logachev, Y. I., Vashenyuk, E. V., et al. 2015, Izv. Ross. Akad. Nauk, Ser. Fiz., 79, 627
Belov, A., Garcia, H., Kurt, V., et al. 2005, CosRe, 43, 165
Bougeret, J. L., Kaiser, M. L., Kellog, P., et al. 1995, SSRv, 71, 231
Chandra, R., Gopalswamy, N., Makela, P., et al. 2013, AdSpR, 52, 2102
Cliver, E. W. 2009, CEAB, 33, 253
Diego, P., Storini, M., & Laurenza, M. 2010, JGR, 115, A06103
Dierckxsens, M., Tziotziou, K., Dalla, S., et al. 2015, SoPh, 290, 841
Duffin, R. T., White, S. M., Ray, P. S., & Kaiser, M. L. 2015, JPhCS, 642, 012006
Garcia, H. A. 1994, ApJ, 420, 422
Gopalswamy, N. 2012, in AIP Conf. Proc. 1500, Energetic Particle and Other Space Weather Events of Solar Cycle 24, ed. Q. Hu et al. (Melville, NY: AIP), 14
Gopalswamy, N., Akiyama, S., Yashiro, H., et al. 2014a, EP&S, 66, 104
Gopalswamy, N., Akiyama, S., Yashiro, S., et al. 2014b, GeoRL, 41, 2673
Gopalswamy, N., Akiyama, S., Yashiro, S., Michalek, G., & Lepping, R. P. 2008, JASTP, 70, 245
Gopalswamy, N., Mäkelä, P., Akiyama, S., Yashiro, S., & Thakur, N. 2015, SunGe, 10, 111
Gopalswamy, N., Mäkelä, P., Yashiro, S., et al. 2015, JPhCS, 642, 012012
Harvey, K. L., & White, O. R. 1999, JGR, 104, 19759
Huang, X., Wang, H.-N., & Li, L.-P. 2012, RAA, 12, 313
Kahler, S. W., Cliver, E. W., & Ling, A. G. 2007, JASTP, 69, 43
Kahler, S. W., & Ling, A. 2015, SpWea, 665, 13
Kahler, S. W., Shea, M. A., Smart, D. F., & Cliver, E. W. 1991, Proc. ICRC 3, (Dublin: The Institute for Advanced Studies), 21
Kontogiannis, I., Belehaki, A., Tsiropoula, G., et al. 2016, AdSpR, 57, 418
Laurenza, M., Cliver, E. W., Hewitt, J., et al. 2009, SpWea, 7, S04008
Laurenza, M., Hewitt, J., Cliver, E. W., Storini, M., & Ling, A. 2007, in 20th Eur. Cosmic Ray Symp. Solar Energetic Proton Events and Soft X-ray Flares, http://www.lip.pt/events/2006/ecrs/proc/ecrs06-s1-34.pdf
McCullagh, P., & Nelder, J. A. 1983, Generalized Linear Models (London: Chapman and Hall) ch. 4
Núñez, M. 2011, SpWea, 9, S07003
Nymmik, R. A. 1999, Rad. Meas., 30, 287
Otkidychev, P. A., & Skorbezh, N. N. 2014, Ge&Ae, 54, 1014
Papaioannou, A., Anastasiadis, A., Sandberg, I., et al. 2015, JPhCS, 632, 012075
Papaioannou, A., Sandberg, I., Anastasiadis, A., et al. 2016, J. Space Weather Space Clim., 6, A42
Park, J., Moon, Y. J., & Gopalswamy, N. 2012, JGR, 117, A08108
Posner, A. 2007, SpWea, 5, S05001
Prasanna Subramanian, S., & Shanmugaraju, A. 2016, Ap&SS, 361, 78
Reames, D. V. 1999, SSRv, 90, 413
Richardson, I. 2013, J. Space Weather Space Clim., 3, A08
Richardson, I., von Rosenvinge, T. T., Cane, H. V., et al. 2014, SoPh, 289, 3059
Signoretti, F., Laurenza, M., Marcucci, M. F., & Storini, M. 2011, Proc. ICRC (Beijing), 267
Silverman, B. W. 1998, Monographs on Statistics and Applied Probability (Boca Raton, FL: CRC Press)
Singh, A. K., & Tonk, A. 2014, Ap&SS, 353, 367
Smart, D., Shea, M., Spence, H. E., & Kepko, L. 2006, AdSpR, 37, 1734
Smart, D. F., & Shea, M. A. 1989, AdSpR, 9, 281
Storini, M., Cliver, E. W., Laurenza, M., & Grimani, C. 2008, OPOCE Publisher for COST 724 Action (Luxembourg: OPOCE), 63–9
Wang, Y.-M., & Colaninno, R. 2014, ApJL, 784, L27
Winter, L. M., & Ledbetter, K. 2015, ApJ, 809, 105